Testing keV sterile neutrino dark matter in future direct detection experiments

Miguel D. Campos[*] and Werner Rodejohann[†]

Max-Planck-Institut für Kernphysik, Saupfercheckweg 1, 69117 Heidelberg, Germany
(Received 18 May 2016; published 7 November 2016)

We determine constraints on sterile neutrino warm dark matter through direct detection experiments, taking XENON100, XENON1T, and DARWIN as examples. If keV-scale sterile neutrinos scatter inelastically with bound electrons of the target material, an electron recoil signal is generated. This can be used to set limits on the sterile neutrino mass and its mixing with the active sector. While not competitive with astrophysical constraints from x-ray data, the constraints are the first direct laboratory bounds on sterile neutrino warm dark matter and will be in some parts of parameter space the strongest limits on keV-scale neutrinos.

I. INTRODUCTION

Dark matter (DM) contributes 5 times more to the energy budget of the Universe than ordinary matter [1]. While first hints of the existence of DM emerged more than 80 years ago [2], its nature has remained elusive, and despite intense effort in the scientific community (both theoretical and experimental), scarce progress has been achieved to settle the issue. Since modifications of gravity cannot explain the evidence for DM on all length and time scales, the generally accepted approach to the DM problem is that particle physics lies at its origin. There is, however, no lack of candidates, the most popular ones belonging in the class of cold dark matter (CDM), whose properties are in convincing agreement with structure formation at large scales [3]. The most frequently considered CDM candidates are weakly interacting massive particles (WIMPs), which are motivated by many theories beyond the Standard Model of particle physics and can generate the right abundance of DM in a straightforward way. Indeed, a large number of dedicated direct detection experiments [4] search for the nuclear recoil from WIMP-nucleon scattering. Apart from such direct detection, indirect detection is possible by looking for signals of decay or annihilation of DM particles in astrophysical observations. The third way of looking for cold dark matter particles is to produce them in collider experiments. A recent review of the various DM candidates, search principles, and the current experimental situation can be found in Ref. [5].

However, some tension has arisen in the last decade with observations at small galaxy formation scales known as the cusp-core problem [6], the missing satellite problem [7], and the too-big-to-fail problem [8]. This has motivated many studies on warm dark matter (WDM) particles, whose properties lead to similar structure formation on large scales but due to a longer free-streaming length to less

structure at smaller ($\lesssim 0.1$ MPc) scales [9]. The most prominent WDM candidates are sterile neutrinos with masses of several keV and very small mixing with active neutrinos. Such sterile neutrinos might, thus, be connected to the mass generation of light active neutrinos [10,11]. Various possibilities for the generation of the WDM density are possible, e.g., via vacuum oscillations [12] or resonant oscillations with the help of lepton asymmetries [13]; see [14] for more discussion. We will not specify any production mechanism here. Indirect searches are possible as their electroweak decay generates characteristic x-ray signals (it is worth mentioning that hints for an unidentified line at about 3.5 keV [15,16] are currently under active discussion and investigation). This approach is the analogue of the indirect detection method for WIMPs mentioned above. The production of keV neutrinos in β decays is another possibility [17] to search for those WDM candidates; this is the analogue of WIMP collider searches.

In this paper, we will show that obtaining *direct detection limits* on keV WDM sterile neutrinos is possible in experiments originally aimed at direct CDM or WIMP detection: if the sterile neutrino mixes with active neutrinos and, thus, scatters inelastically with bound electrons of the target material, the scattered electrons create electron recoils which some of the direct detection experiments can detect. We use data from the XENON100 experiment to set the first direct detection limits on keV neutrino WDM and present the prospects for the upcoming XENON1T, XENONnT, and DARWIN experiments. Those bounds are not compatible with indirect astrophysical bounds, but will be the only direct detection limits, and in some parts of parameter space the best limits on sterile neutrinos, assuming, of course, that they form the wholeness of dark matter and mix with electron neutrinos.

II. DIRECT DETECTION OF DARK MATTER

Direct detection experiments are suited for WIMP physics through their coherent scattering with a nucleus

---
[*]miguel.campos@mpi-hd.mpg.de
[†]werner.rodejohann@mpi-hd.mpg.de

and observing the generated nuclear recoil. Constraints are set on interaction cross section and DM mass, and currently the direct detection experiments setting the most stringent limits for masses above ~5 GeV are XENON100 [18], LUX [19], and Panda-X [20] involving several dozen kilograms of liquid xenon. We will focus in what follows on the former experiment, whose next step is called XENON1T [21], involving 1 ton fiducial volume; an even bigger stage would be XENONnT. We will also estimate the effects in the future DARWIN experiment [22] that will aim at a 100-fold increase in exposure (and sensitivity to spin-independent WIMP-nucleus interaction) compared to XENON1T. The detection principle (for a general overview, see [4]) of these dual phase detectors is that the deexcitation of secondary xenon atoms that have interacted with the primary scattered atom lead to a prompt scintillation signal (called S1). Ionization electrons are extracted in the gas phase part of the instrument via electric fields and create another light signal (S2) via scintillation. For WIMP searches, electron recoils (ERs) represent a source of background. They can be produced by the scattering of photons or electrons with the electron cloud surrounding the xenon nucleus, and the sources include intrinsic β decays of element traces present in xenon (such as ^{222}Rn and ^{85}Kr) and gamma rays crossing the shielding. As ERs and nuclear recoils have different ratios of S1 and S2, it is possible to impose cuts to exclude ERs. However, when one thinks beyond the WIMP possibility, ERs are interesting on their own and allow us to probe physics beyond standard WIMPs. Indeed, dedicated analyses of the XENON100 Collaboration have studied axions [23] and DM particles interacting purely with electrons [24]. We use here the results from [23] to set constraints on keV-scale sterile neutrino dark matter and will also give limits on the relevant parameters for future stages of the experiment.[1] To be able to use the ER data coming from direct detection experiments, it is necessary that the signal produced by the DM candidate exceeds the background in some energy interval. As we will see, it is possible to generate the required excess when we consider WDM sterile neutrinos in the keV range. We use the background model coming from calibration data for ER in XENON100 [23]. For the case of XENON1T, we will scale this background model such that it reproduces the background of $\sim 1.8 \times 10^{-4}$ (kg day keV)$^{-1}$ predicted in [21] for XENON1T. We will also use the predictions from [22, 25] to estimate the effect in the DARWIN experiment. As a comparison, the average background in DARWIN is estimated to be $\sim 2.05 \times 10^{-5}$ (kg day keV)$^{-1}$ using an extrapolation of Fig. 2 (right) in [25].

---

[1]Let us note that other current or future experiments with sensitivity for electron recoils such as CDMS, CRESST, EDELWEISS, LZ, or XMASS can also provide interesting limits.

The process analyzed is based on the inelastic charged and neutral scattering $N_S e^- \rightarrow \nu_e e^-$ (and $N_S e^- \rightarrow \bar{\nu}_e e^-$), where a WDM sterile neutrino N_S mixing with an active state scatters an electron from a xenon atom. Its velocity in the standard halo model is $v(N_S) \simeq 220$ km/s $[\beta = \mathcal{O}(10^{-3})]$, and, hence, its energy essentially equals its mass, $E_S \simeq m_S$. The cross section for the process in the case of free electrons at rest [i.e., $p_e = (m_e, \vec{0})$ for the electron at rest and $p'_e = (m_e + E_k, \vec{p}_e)$ for the scattered one] is

$$\frac{d\sigma_{\text{free}}}{dE_k} = 2\frac{G_F^2}{\pi}|U_{Se}|^2 \frac{m_e}{|\vec{p}_S|^2}\left[g_1^2 E_S\left(E_S + \frac{m_S^2}{2m_e}\right) \right.$$
$$+ g_2^2(E_S - E_k)\left(E_S - E_k + \frac{m_S^2}{2m_e}\right)$$
$$\left. - g_1 g_2\left(m_e E_k + \frac{1}{2}m_S^2\right)\right]. \tag{1}$$

The total cross section is the sum of the $\nu_e e^-$ and $\bar{\nu}_e e^-$ final states and is dominated by the $\nu_e e^-$ channel. We have defined

$$g_1^\nu = g_2^{\bar{\nu}} := 1 + \frac{1}{2}(g_V + g_A),$$
$$g_2^\nu = g_1^{\bar{\nu}} := \frac{1}{2}(g_V - g_A),$$

with $g_V = -\frac{1}{2} + 2\sin^2\theta_W$ and $g_A = -\frac{1}{2}$. The reaction, as in all sterile neutrino processes, is suppressed due to the mixing angle between sterile and active neutrinos $|U_{S\alpha}|^2$. We note that Ref. [26] has considered coherent inelastic WDM-atom scattering of a 5 keV sterile neutrino, not taking the effect of bound electrons into account. In contrast, we will consider here sterile neutrinos in the range $\mathcal{O}(10$–$50)$ keV, corresponding to a wavelength of $\mathcal{O}(10^{-8}$–$10^{-9})$ cm. As the radius of a xenon atom is $\sim 1.1 \times 10^{-8}$ cm, the electron-neutrino scattering is incoherent, and all the bound electrons in the xenon atom must be considered. As scattering with bound electrons leads to larger recoil than the free case (see Fig. 1), this is actually crucial to our analysis. One of the reasons this is important is because when considering just free electrons one would need masses higher than ~20 keV to go beyond the minimum threshold of the detector, discussed later, hence, entering the incoherent regime. To evaluate the electron recoil cross section with these bound electrons, we have performed the calculation in a similar way as it was done in Ref. [27], suitably modified to take the non-negligible incoming neutrino mass into account. An effective mass for the bound electron is defined as $\tilde{m} := E_B^2 - |\vec{p}_B|^2 \equiv E_B^2 - p_B^2$, where the bound electron has momentum $\vec{p}_B$ and energy $E_B = m_e - \varepsilon$, ε being the binding energy. All atomic wave functions have been considered using the
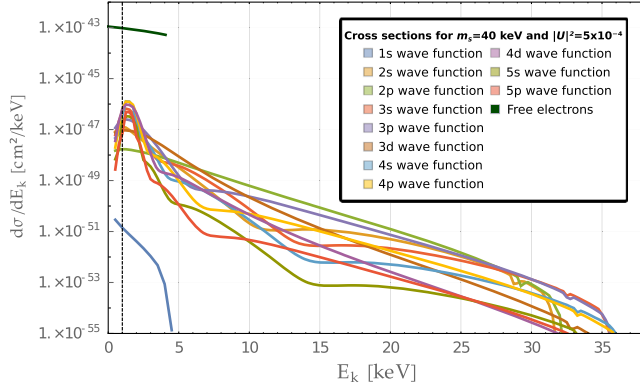
FIG. 1. Differential cross section of massive sterile neutrinos with free (dark green) and bound electrons (light colors) for $m_S = 40$ keV and $|U_{Se}|^2 = 5 \times 10^{-4}$. Dashed vertical line represents lower threshold of $E_{\text{Th}} = 1$ keV (see next section).

Roothann-Hartree-Fock method, with data coming from Ref. [28]. It is worth to mention that neither electron spin nor relativistic effects were taken into account in this expansion. It is suggested in [27] that errors for the most loosely bound electronic states could be up to 10% due to spin effects. The differential cross section for an electron in a state t $(t = 1s, 2s, 2p, …)$ in the rest frame of the atom where (p_B, θ, ϕ) are the variables of the bound electron is obtained through

$$\frac{d\sigma_t}{dE_k} = \int \frac{p_B^2 dp_B d(\cos\theta) d\phi}{(2\pi)^3} \frac{|R_t(\vec{p}_B)|^2}{4\pi}$$
$$\times \frac{|\mathcal{M}|^2}{4E_S E_B |\beta - p_B/\tilde{m}|} \left| \frac{1}{8\pi\lambda^{1/2}(s, m_S^2, \tilde{m}^2)} \right| \frac{du}{dE_k} \right|. \quad (2)$$

Here, $R_t(\vec{p}_B)$ are the radial wave functions of the bound electrons defined in [27] and normalized such that

$$\int_0^\infty \frac{k^2 dk}{(2\pi)^3} |R_t(k)|^2 = 1. \quad (3)$$

The function $\lambda(a, b, c) := a^2 + b^2 + c^2 - 2ab - 2bc - 2ca$ is the Källén function, and s and u are the usual Mandelstam variables. As an example, the differential cross section for free and bound electrons in the different shells is presented in Fig. 1 for a given choice of parameters, namely, $m_S = 40$ keV and $|U_{Se}|^2 = 5 \times 10^{-4}$. As we can see in Eq. (2), the differential cross section involves an integration in p_B. The upper limit for this variable is obtained from the allowed range of the final state particles as it was done in [29], which contains the threshold condition for the process to occur in the different bound states (i.e., $E_S > \varepsilon_t$). The limits on E_k were obtained from [27], but they are equivalent to those presented in [29]. These limits are dependent on ε_t, a fact reflected in Fig. 1 where the most tightly bound electron ($\varepsilon_{1s} = 34.561$ keV)

has a differential cross section with a narrow allowed range in E_k in strong contrast to the more loosely bound states ($\varepsilon_{2s} = 5.453$ keV, $\varepsilon_{2p} = 4.893$ keV, …).

We can obtain the differential event rate of the process, in units of $(\text{kg day keV})^{-1}$,

$$\frac{dR_t}{dE_k}(m_S, |U_{Se}|^2) = \frac{\rho_0}{m_S} n_e \int \frac{d\sigma_t}{dE_k}(m_S, |U_{Se}|^2) f(\beta)\beta d\beta. \quad (4)$$

Here, ρ_0 is the local DM density, n_e the number of electrons per kilogram of target material, and $f(\beta)$ is the velocity distribution in the detector frame. In general, different DM production mechanisms lead to different distribution functions; however, one can safely assume that this distribution has evolved with time, leading to a DM halo with a (truncated in $v_{\text{esc}} = 544$ km/s) Maxwell-Boltzmann distribution centered in $v_c = 220$ km/s as it is done in the standard halo model.[2]

If T is the exposure time and M the mass of the detector, we can finally define the differential number of events corresponding to a particular electronic configuration:

$$\frac{dN_t}{dE_k}(m_S, |U_{Se}|^2) = MT \frac{dR_t}{dE_k}(m_S, |U_{Se}|^2). \quad (5)$$

For XENON100 and XENON1T, we take, respectively,

$$M_{100} = 34 \text{ kg} \quad \text{and} \quad T_{100} = 224.6 \text{ days},$$
$$M_{1T} = 10^3 \text{ kg} \quad \text{and} \quad T_{1T} = 2 \times 365 \text{ days}. \quad (6)$$

Notice that in the case of XENONnT, a global factor n appears in comparison with XENON1T. Several experimental aspects will probably be slightly different from the case of XENON1T and cannot be reliably stated at the moment. The analysis for XENONnT has not been included here due to these reasons, but the limits can roughly be estimated to scale with n. For the DARWIN case, we will use an exposure of $MT = 200$ ton yr as in [22].

III. ANALYSIS AND RESULTS

We perform now an analysis to estimate the parameter range for the variables $(m_S, |U_{Se}|^2)$ that can be excluded using a direct detection experiment. To be able to evaluate the differential number of events and compare it with the background, it is necessary to take into consideration the global acceptance of the detector for ER, Acc(PE), which is specially important in the low energy range and depends on the number of photoelectrons (PEs) measured in S1.

---

[2]As the analysis follows the usual WIMP strategy, effects such as annual modulation are, in principle, also observable but are neglected here.

Equally important is the conversion function $\mathrm{Conv}(E_k)$ that takes into account the scintillation efficiency and the quenching factor and relates the measured PE with the recoil energy of the scattered electrons E_k. The ER acceptance and the conversion function in XENON1T are considered to be the same as for XENON100, both extracted from [23]. This is a conservative approach considering that XENON1T expects to increase the light collection in comparison with XENON100 [21]. The differential number of events is then

$$\frac{dN_T}{dE_k}(m_S, |U_{Se}|^2) = \sum_t \mathrm{Acc}(\mathrm{Conv}(E_k)) n_t \frac{dN_t}{dE_k}(m_S, |U_{Se}|^2),$$

where n_t is the number of electrons in the t state. Any given values of the mass of the sterile neutrino m_S and the mixing angle $|U_{Se}|^2$ generate a particular shape for the differential number of events in terms of the kinetic energy of the scattered electron E_k. This is shown in Fig. 2 using $m_S = 40$ keV and $|U_{Se}|^2 = 5 \times 10^{-4}$ for XENON1T; the background is also shown.

We restrict the analysis to the case in which the signal is entirely above the background and integrate to define

$$N_s := \int_{E_{\mathrm{Th}}}^{E_0} \frac{dN_T}{dE_k} dE_k \quad \text{and} \quad N_b := \int_{E_{\mathrm{Th}}}^{E_0} F_b dE_k. \quad (7)$$

Here, E_{Th} is a lower energy threshold, which is set to 2 keV for XENON100 and 1 keV for XENON1T (this threshold is shown as a dashed black line in Figs. 1 and 2). $E_0(m_S)$ is the point in which the signal $\frac{dN_T}{dE_k}$ intersects the background F_b, otherwise, it is simply the upper bound of the electron energy allowed by kinematical constraints. For the DARWIN case, the background was extracted from [25] and extrapolated to the region of interest. The lower threshold and the acceptance function considered will be assumed as in the XENON1T case.
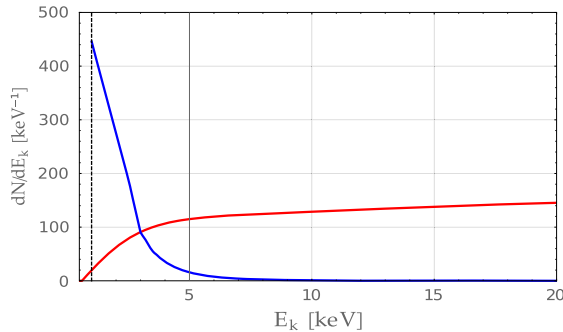

FIG. 2. Differential number of events for bound electrons for $m_S = 40$ keV and $|U_{Se}|^2 = 5 \times 10^{-4}$ in XENON1T (blue) and estimated background F_b (red). Dashed vertical line represents lower threshold of $E_{\mathrm{Th}} = 1$ keV.

From this block space analysis we define the significance in terms of a χ^2 distribution as a function of N_s and N_b,

$$\chi^2(m_S, |U_{Se}|^2) := \frac{(N_s(m_S, |U_{Se}|^2) - N_b(m_S, |U_{Se}|^2))^2}{N_b(m_S, |U_{Se}|^2)}.$$

$$(8)$$

Imposing that $\chi^2 \geq 4.60$ (13.82) for 90% (99.9%) C.L., we obtain the region in terms of m_S and $|U_{Se}|^2$ that can be excluded.

Using the live time shown in Eq. (6) for XENON100 and XENON1T, we obtain the light and dark green regions shown in Fig. 3. Notice that when compared to XENON1T, due to a larger background, higher threshold, and a smaller value of $M \ T$, $|U_{Se}|^2$ must be $\sim \mathcal{O}(10^2)$ times larger to achieve the same effect in XENON100. In fact, for XENON100 the excluded area has been already excluded in other Earth-based experiments. However, XENON1T can set interesting limits on the parameters and is much closer to detection than the capture of keV-scale WDM neutrinos in β-decaying nuclei [30]. Additionally, using an
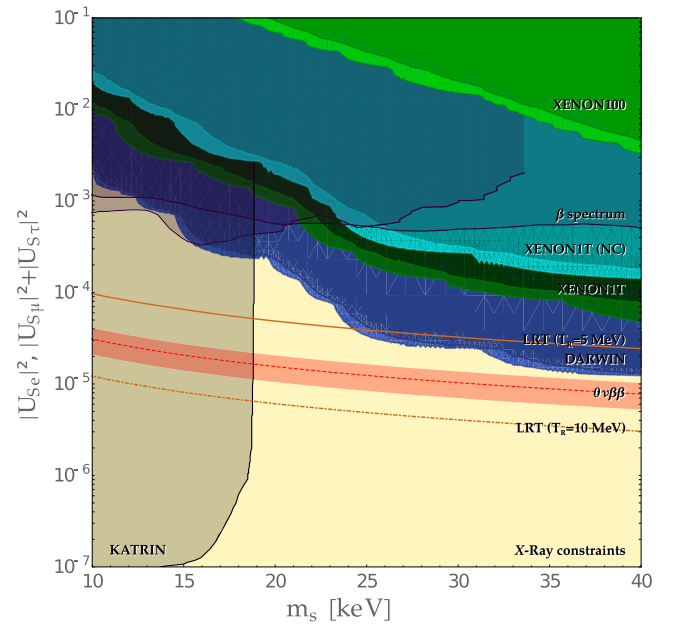

FIG. 3. Light green: Sensitivity on sterile neutrino WDM parameters for XENON100 as a function of m_S and $|U_{Se}|^2$. The contours delimit 90% and 99.9% C.L. Dark green: Equivalent for XENON1T. Blue: Equivalent for DARWIN. Purple: Current limits from analysis of β spectrum of different radioisotopes [31,32]. Black: Expected statistical sensitivity of a modified KATRIN setup (Fig. 11 in [17]). Red dashed: Limits coming from $0\nu\beta\beta$ experiments [33]. Orange solid (and dot-dashed): Excluded area for production in case of a low reheating temperature (LRT) of $T_R = 5$ MeV ($T_R = 10$ MeV) [36]. Yellow: Constraint from x-ray searches [39,40]. Turquoise denoted "XENON1T (NC)": Limit on $|U_{S\mu}|^2 + |U_{S\tau}|^2$ if the sterile neutrino does not couple to electron neutrinos and only has neutral currents.

exposure of 200 ton yr for the DARWIN experiment we obtain the blue curve, which is a bit less than an order of magnitude better than the XENON1T case. As a comparison, we show in the same figure the current exclusion limits for different Earth-based experiments in purple in which the β spectrum of ^{63}Ni [31] and ^{35}S [32] was analyzed. The black area is the expected 90% statistical exclusion limit of a differential measurement of three years with a modified setup of the KATRIN experiment [17]. It would be several orders of magnitude more sensitive in the mixing angle, but the mass range is more limited. The red dashed line represents the limit using the null results from neutrinoless double beta decay ($0\nu\beta\beta$) experiments with the constraint $|U_{Se}|^2 m_S < (0.3 \pm 0.1)$ eV; see, for example, [33]. This limit is almost 1 order of magnitude more sensitive in comparison to XENON1T but assumes that the neutrinos are Majorana particles (as in relic neutrino capture [34] there will be a factor 2 smaller cross section for Dirac neutrinos) and that none of the many possible mechanisms for double beta decay interferes. For the shown mass range, the Dodelson-Widrow mechanism [12] to produce the dark matter abundance sets a limit for $|U_{Se}|^2$ below 10^{-9}, as derived in [35]. This mechanism in which the relic abundance is produced through the oscillation of active to sterile states in the early Universe is unavoidable, which means that if the $(m_S, |U_{Se}|^2)$ parameter space is in reach of the XENON1T or the DARWIN experiment, this would call for an alternative explanation for an otherwise overproduced relic abundance (apart from having a too short lifetime). One possibility is, for example, to consider a low reheating temperature in inflationary models which would suppress the production of nonrelativistic particles at $T \lesssim T_R$ [36]. The excluded area for $T_R = 5$ MeV (and $T_R = 10$ MeV) is shown in orange (and dot-dashed orange), and limits from XENON1T can be comparable. Another option is to assume the insertion of additional entropy in the system, as, e.g., in Refs. [37,38]. The yellow area shows current astrophysical x-ray constraints [39,40]. Finally, if the sterile neutrino does not couple to the electron neutrino, it can still have neutral current reactions.

The (weaker) limit on $|U_{S\mu}|^2 + |U_{S\tau}|^2$ is also shown in the plot in turquoise. The limits from beta and double beta decay do not apply here.

We can see that while astrophysical x-ray limits will remain the strongest bounds, the exclusion limit for the mixing angle with the electron neutrino obtained for current direct detection experiments can be up to 1 order of magnitude stronger in comparison with other Earth-based limits and up to 2 orders of magnitude using future experiments.

IV. CONCLUSIONS

In this work, we have proposed a method to extract sensitive information on sterile neutrino warm dark matter from electron recoil data in direct detection experiments. This has resulted in a way to constrain the mixing angle $|U_{Se}|^2$ and the sterile neutrino mass m_S independently of cosmological exclusion limits and complementary to them. The constrained values of mass and mixing would in standard scenarios imply a too large dark matter density, and interesting and far-reaching nonstandard scenarios would be needed in order to reconcile with observation. Considering two years of live time for the XENON1T experiment, the mass range, which is possible to exclude using the method analyzed, is between 10 and 40 keV, while the limit on the square of the mixing angle can go down to $\sim 5 \times 10^{-5}$. On the other hand, when the exposure is increased 2 orders of magnitude, as in the case of the DARWIN experiment, the mixing angle squared can be constrained down to 10^{-5}.

[1] P. A. R. Ade *et al.* (Planck Collaboration), Astron. Astrophys. **594**, A13 (2016).
[2] F. Zwicky, Helv. Phys. Acta **6**, 110 (1933).
[3] V. Springel *et al.*, Nature (London) **435**, 629 (2005).
[4] T. Marrodán Undagoitia and L. Rauch, J. Phys. G **43**, 013001 (2016).
[5] M. Klasen, M. Pohl, and G. Sigl, Prog. Part. Nucl. Phys. **85**, 1 (2015).
[6] R. F. G. Wyse and G. Gilmore, IAU Symp. **244**, 44 (2008).
[7] B. Moore, S. Ghigna, F. Governato, G. Lake, T. Quinn, J. Stadel, and P. Tozzi, Astrophys. J. **524**, L19 (1999).
[8] M. Boylan-Kolchin, J. S. Bullock, and M. Kaplinghat, Mon. Not. R. Astron. Soc. **415**, L40 (2011).
[9] A. Boyarsky, J. Lesgourgues, O. Ruchayskiy, and M. Viel, J. Cosmol. Astropart. Phys. 05 (2009) 012.
[10] L. Canetti, M. Drewes, T. Frossard, and M. Shaposhnikov, Phys. Rev. D **87**, 093006 (2013).
[11] K. N. Abazajian *et al.*, arXiv:1204.5379.

[12] S. Dodelson and L. M. Widrow, Phys. Rev. Lett. **72,** 17 (1994).

[13] X.-D. Shi and G. M. Fuller, Phys. Rev. Lett. **82,** 2832 (1999).

[14] A. Kusenko and L. J. Rosenberg, arXiv:1310.8642.

[15] E. Bulbul, M. Markevitch, A. Foster, R. K. Smith, M. Loewenstein, and S. W. Randall, Astrophys. J. **789,** 13 (2014).

[16] A. Boyarsky, O. Ruchayskiy, D. Iakubovskyi, and J. Franse, Phys. Rev. Lett. **113,** 251301 (2014).

[17] S. Mertens, T. Lasserre, S. Groh, G. Drexlin, F. Glück, A. Huber, A. W. P. Poon, M. Steidl, N. Steinbrink, and C. Weinheimer, J. Cosmol. Astropart. Phys. 02 (2015) 020.

[18] E. Aprile *et al.* (XENON100 Collaboration), arXiv:1609.06154.

[19] D. S. Akerib *et al.*, arXiv:1608.07648.

[20] A. Tan *et al.* (PandaX-II Collaboration), Phys. Rev. Lett. **117,** 121303 (2016).

[21] E. Aprile *et al.* (XENON Collaboration), J. Cosmol. Astropart. Phys. 04 (2016) 027.

[22] J. Aalbers *et al.* (DARWIN Collaboration), arXiv:1606.07001.

[23] E. Aprile *et al.* (XENON100 Collaboration), Phys. Rev. D **90,** 062009 (2014).

[24] E. Aprile *et al.* (XENON100 Collaboration), Science **349,** 851 (2015).

[25] M. Schumann, L. Baudis, L. Bütikofer, A. Kish, and M. Selvi, J. Cosmol. Astropart. Phys. 10 (2015) 016.

[26] S. Ando and A. Kusenko, Phys. Rev. D **81,** 113006 (2010).

[27] G. J. Gounaris, E. A. Paschos, and P. I. Porfyriadis, Phys. Rev. D **70,** 113008 (2004).

[28] C. F. Bunge, J. A. Barrientos, and A. V. Bunge, At. Data Nucl. Data Tables **53,** 113 (1993).

[29] W. Liao, X.-H. Wu, and H. Zhou, Phys. Rev. D **89,** 093017 (2014).

[30] Y. F. Li and Z.-z. Xing, Phys. Lett. B **695,** 205 (2011).

[31] E. Holzschuh, W. Kundig, L. Palermo, H. Stussi, and P. Wenk, Phys. Lett. B **451,** 247 (1999).

[32] E. Holzschuh, L. Palermo, H. Stussi, and P. Wenk, Phys. Lett. B **482,** 1 (2000).

[33] W. Rodejohann, Int. J. Mod. Phys. E **20,** 1833 (2011).

[34] A. J. Long, C. Lunardini, and E. Sabancilar, J. Cosmol. Astropart. Phys. 08 (2014) 038.

[35] T. Asaka, M. Laine, and M. Shaposhnikov, J. High Energy Phys. 01 (2007) 091; 02 (2015) 028(E).

[36] G. Gelmini, S. Palomares-Ruiz, and S. Pascoli, Phys. Rev. Lett. **93,** 081302 (2004).

[37] F. Bezrukov, H. Hettmansperger, and M. Lindner, Phys. Rev. D **81,** 085032 (2010).

[38] M. Nemevsek, G. Senjanovic, and Y. Zhang, J. Cosmol. Astropart. Phys. 07 (2012) 006.

[39] S. Horiuchi, P. J. Humphrey, J. Onorbe, K. N. Abazajian, M. Kaplinghat, and S. Garrison-Kimmel, Phys. Rev. D **89,** 025017 (2014).

[40] A. Kusenko, Phys. Rep. **481,** 1 (2009).